Traffic 2012; **13:** 338–354

doi:10.1111/j.1600-0854.2011.01303.x

Evidence for Sequential Action of Rab5 and Rab7 GTPases in Prevacuolar Organelle Partitioning

Francesca Bottanelli[1], David C. Gershlick and Jürgen Denecke*

Centre for Plant Sciences, Faculty of Biological Sciences, University of Leeds, Leeds, LS2 9JT, UK
[1]Present address: Department of Cell Biology, Yale University, School of Medicine, New Haven, CT 06520-8002, USA

**Corresponding author: Jürgen Denecke, j.denecke@leeds.ac.uk*

GTPases of the Rab5 and Rab7 families were shown to control vacuolar sorting but their specific subcellular localization is controversial in plants. Here, we show that both the canonical as well as the plant-specific Rab5 reside at the newly discovered 'late prevacuolar compartment' (LPVC) while Rab7 partitions to the vacuolar membrane when expressed at low levels. Higher expression levels of wild-type Rab5 GTPases but not Rab7 lead to dose-dependent inhibition of biosynthetic vacuolar transport. In the case of Ara6, this included aberrant co-localization with markers for earlier post-Golgi compartments including the *trans*-Golgi network. However, nucleotide-free mutants of all three GTPases (Rha1, Ara6 and Rab7) cause stronger dose-dependent inhibition of vacuolar sorting. In addition, nucleotide-free Rha1 led to a later maturation defect and co-localization of markers for the prevacuolar compartment (PVC) and the LPVC. The corresponding Rab7 mutant strongly inhibited vacuolar delivery without merging of PVC and LPVC markers. Evidence for functional differentiation of the Rab5 family members is underlined by the fact that mutant Rha1 expression can be suppressed by increasing wild-type Rha1 levels while mutant Ara6 specifically titrates the nucleotide exchange factor Vps9. A model describing the sequential action of Rab5 and Rab7 GTPases is presented in the light of the current observations.

Key words: Guanine nucleotide exchange factor, late prevacuolar compartment, organelle maturation, prevacuolar compartment, protein trafficking, Rab GTPase, vacuolar sorting

Received 15 March 2011, revised and accepted for publication 14 October 2011, uncorrected manuscript published online 18 October 2011, published online 21 November 2011

Vacuoles are terminal organelles of the secretory pathway and perform a multiplicity of functions from waste disposal, maintenance of turgor pressure to storage of proteins (1). Protein sorting to the plant vacuole is well known to be a receptor-mediated process (2–6). The most recent transport model suggests that vacuolar sorting receptors (VSRs) are salvaged from the prevacuolar compartment (PVC) in a signal-mediated process to avoid vacuolar degradation (7). Continuous depletion of receptors causes enrichment of vacuolar cargo and thus maturation to a later compartment called the late prevacuole (LPVC). Although the exact mechanism controlling PVC to LPVC maturation and the underlying machinery have yet to be elucidated, it is likely that Rab5 GTPase family members are involved. Although mammalian Rab5 GTPases have an established role in endocytosis (8), various studies in plants suggest a predominant role in biosynthetic trafficking to the vacuole (9–11). We have recently obtained evidence for a role of Rab7 in vacuolar protein sorting (12). However, conflicting reports suggest that this GTPase is either localized to the vacuolar membrane (13) or to endosomes (14).

Unlike mammalian cells and yeast, plants contain two classes of Rab5 GTPases. Rha1 and Ara7 represent the canonical C-terminally lipid anchored GTPases and show very high sequence homology against each other (9). In contrast, Ara6 is a plant unique Rab5 which is characterized by N-terminal myristoylation as well as significant sequence divergence compared to the other two members (15,16). Fluorescently tagged Rab5 members were earlier localized to endosomal compartments (10,11,15,17,18). Ueda and colleagues suggested a functional differentiation of the two Rab5 classes as Ara6 and Ara7 localized to overlapping but not identical endosomal populations (18,19). In support of this hypothesis, a knock-out mutant of the Rab5 GEF vps9 was differentially complemented by GTP-locked Ara7 but not Ara6 (20). Immunogold localization analysis of all the Rab5 family members consistently revealed labelling of multivesicular structures (21), but it is possible that these consist of different populations as in mammalian cells both early and late endosomes have a multivesicular appearance (22).

We have recently shown that one plant Rab5 member (Rha1/RabF2a) specifically enriches at the LPVC, rather than the PVC. In this study, we show that both canonical and plant-specific Rab5 members localize to this late compartment while Rab7 specifically labels the tonoplast and intravacuolar bulbs. Despite residing in the same organelle, the two Rab5 classes appear to act in a differential manner and may thus control distinct transport events. Moreover, the subcellular localization to the most distal membrane in the vacuolar route supports the notion that Rab7 acts downstream of Rab5 in the pathway.

Results

Rab7 partitions to the tonoplast when expressed at low levels

We have recently shown that expression of nucleotide-free Rab7 leads to a drastic retention of soluble vacuolar cargo in post-Golgi punctate structures, most likely because of a late transport defect to the vacuolar membrane. The Rab7 mutant also inhibited vacuolar delivery of the membrane marker GFP-Vam3, in sharp contrast to nucleotide-free Rab5 members which had no effect on this membrane marker (12). Here, we wanted to study the subcellular localization of Rab7 and test if it labels the tonoplast as shown in an earlier report (13), or the endosomes or prevacuoles (14).

First experiments in tobacco leaf protoplasts using a Cauliflower Mosaic Virus 35S (CaMV35) promoter-driven CFP-fusion to the N-terminus of Rab7 revealed a typical cytosolic expression pattern and was considered to be an overexpression artefact (data not shown). Since Rab7 depends on post-translational modifications to acquire a C-terminal lipid anchor, it is possible that overexpression leads to incomplete modification and unusually high cytosolic levels which prevent accurate subcellular localization studies.

We thus wanted to express the GTPase with the weaker TR2′-promoter (23) which has been successfully used to localize a fluorescent Rab5 fusion to the LPVC (7) or to express low levels of organelle markers to avoid signals of molecules in transit through earlier compartments, such as the ER in the case of the Golgi marker ST-YFP (12). Figure S1A illustrates the drastically reduced expression level of the plasma membrane marker YFP-SYP121 compared to the equivalent fusion to the CaMV35S-promoter, when both chimeric genes were expressed in tobacco leaf epidermis cells transformed via *Agrobacterium tumefaciens*-mediated genomic integration. This qualitative analysis was confirmed via quantitative enzyme essays from 15 independent transgenic tobacco lines expressing the reporter enzyme β-glucuronidases (GUS) under control of either the CaMV35S- or the TR2′-promoter. Figure S1B reveals that the TR2′-promoter yields approximately 10-fold lower GUS expression levels in leaves compared to the CaMV35S promoter.

Figure 1A shows an overview of several leaf epidermis cells expressing variable levels of CFP-Rab7 under control of the TR2′-promoter together with the established tonoplast marker YFP-Vam3. Some cells expressing high levels of CFP-Rab7 were still observed showing strong peripheral cytosolic overexpression (OE) and such cells were not suitable for localization studies. However, the

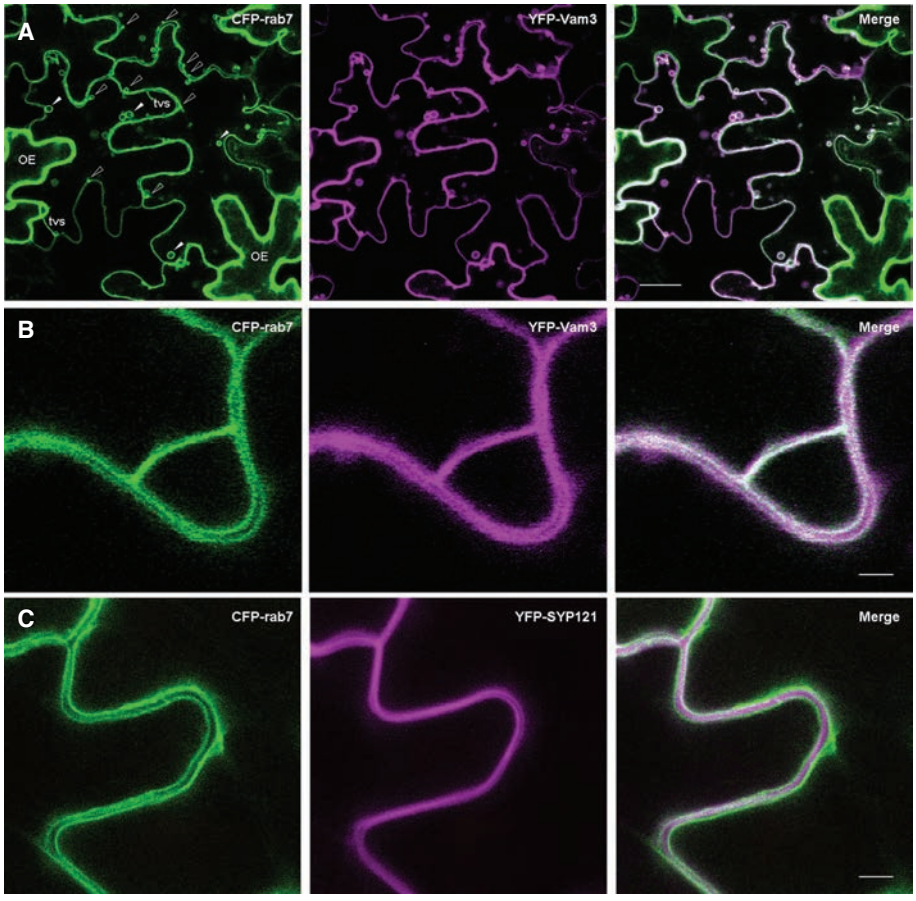

Figure 1: Rab7 partitions to the tonoplast in plants. Infiltrated tobacco leaves expressing CFP fused to the N-terminus of Rab7 together with the tonoplast marker YFP-Vam3 (A,B) or the plasma membrane marker YFP-SYP121 (C). In order to obtain sharp images of membranes at the cell periphery, tissues were scanned with the focal plane in the centre of the epidermis. Notice that CFP-Rab7 (green) labels the same membranes as YFP-Vam3 (purple) including transvacuolar strands and intravacuolar vesicles known as 'bulbs' (white arrows, panel A). Scale bars are 20 μm for panel A and 5 μms for panels B and C.

majority of the cells expressed low levels of CFP-Rab7 and revealed perfect co-localization with the tonoplast marker, labelling the delimiting vacuolar membrane (tonoplast) as well as transvacuolar strands (tvs) and intracellular bulbs (Figure 1A, arrow heads). The latter were of variable size and were either large (solid white arrow heads) or small nascent (open arrow heads) but always on the lumenal side of the vacuolar membrane. In addition, all CFP-Rab7 signals always overlapped those of the tonoplast marker YFP-Vam3 (Figure 1B). Control experiments with co-expressed markers for cytosolic organelles focussing at the cell cortex revealed a homogeneous green fluorescence from CFP-Rab7 originating from the tonoplast underneath. Green punctate structures in the cytosol were not detected under these conditions.

In sharp contrast, co-expression of TR2′-promoter-driven CFP-Rab7 with the TR2′-promoter-driven plasma membrane marker YFP-SYP121 revealed clear segregation of the two fluorescent signals (Figure 1C). The plasma membrane signal of two adjacent cells are closer together compared to the CFP-Rab7-labelled vacuolar membranes that are further separated by additional cytosol in both adjacent cells (compare green and purple channel). In the merged image, a clear purple signal is sandwiched between two green layers.

In conclusion, CFP-Rab7 effectively segregates from the cytosol to the tonoplast when expressed at low levels, while cytosolic expression is correlated with overexpression. All additional membrane structures can be attributed to transvacuolar strands or various types of intravacuolar bulbs.

Ara6-GFP and VENUS-Rha1 localize to the LPVC when expressed at low levels

Given the recent discovery of the LPVC (7), a distinct compartment situated between the PVC and the vacuole and characterized by a high concentration of vacuolar cargo and the Rab5 GTPase Rha1, we wanted to test the localization of the plant-specific Rab5 GTPase Ara6 under similar experimental conditions. For this purpose, an Ara6-RFP chimera was cloned under control of the TR2′-promoter (23) for low expression levels and its localization was analysed in comparison to the canonical Rab5 chimera VENUS-Rha1 (7). Correlation analysis was performed by using the 'Pearson–Spearman correlation' (PSC) plugin for ImageJ (24) to quantify co-localization in a statistically meaningful way (7).

To test if the two Rab5 GTPases co-localize to the same structures or segregate into different populations, tobacco leaves were infiltrated with Agrobacterium strains harbouring the TR2-driven Ara6-RFP and VENUS-Rha1 encoding-plasmids. Figure 2A shows that the two fluorescent protein fusions co-localized to the same structures. The scatterplots reveal a single population of yellow pixels distributed along the diagonal line, resulting in a high correlation coefficient.

In addition, each of the two Rab5 GTPase fusions was co-expressed for markers for the TGN, PVC and LPVC. When co-expressed with fluorescent fusions of the recycling-defective receptor mutant VSR2(L615A) serving as LPVC marker, both Rab5 fusions also showed a high degree of overlap resulting in a predominant yellow population of pixels (Figure 2B, C). The obtained correlation coefficients are lower than in panel A due to VSR2(L615A) being in transit through the PVC (7) which is not labelled by the GTPase Rha1 (arrowheads).

When co-expressed with the PVC-resident wild-type VSR2 fusions, the two GTPases behave in a differential manner. VENUS-Rha1 and RFP-VSR2 showed little overlap resulting in two completely distinct populations of either green (VENUS-Rha1) or red (RFP-VSR2) pixels (Figure 2D). This corresponds to earlier observations (7). In contrast, Ara6-RFP appeared to co-localize stronger with the PVC marker GFP-VSR2 resulting in a significant yellow population (Figure 2E).

Further control experiments involved testing the TGN/Early endosome. When co-expressed with fluorescent Syp61 fusions as TGN marker, neither TR2-driven VENUS-Rha1 nor TR2-driven Ara6-RFP showed any overlap (Figure S2) resulting in negative correlation coefficients.

Overexpression of Rab5 GTPases causes post-Golgi organelle fusion

Although both Rab5 GTPases appeared to label the same structures when co-expressed (Figure 2A), individual expression with the PVC marker VSR2 revealed subtle differences. To verify if overexpression of either GTPases influences organelle maturation, we repeated the experiment with stronger CaMV35S promoter-driven chimeras and subjected the data to the same statistical rigor.

Co-expression studies using the TGN marker revealed that overexpression can alter Rab5 localization and differentially affects the two classes. While Rha1 continued to label structures distinct from the TGN marker (Figure 3A), Ara6-GFP showed significant co-localization with the SNARE chimera YFP-Syp61 (cf. Figure 3B with Figure S2B).

Co-localization with the PVC marker GFP-VSR2 revealed that both Rab5 classes highlighted the same punctate structures (Figure 3C, D), giving rise to a typical diagonal plot of pixels in yellow. This is in contrast to low Rha1 expression levels (Figure 2D) and suggests that overexpression of Rha1 causes a defect in PVC to LPVC maturation. In the case of Ara6, partial PVC localization was already observed with the TR2′ promoter-driven Rab (Figure 2D). This trend is now aggravated when driven by

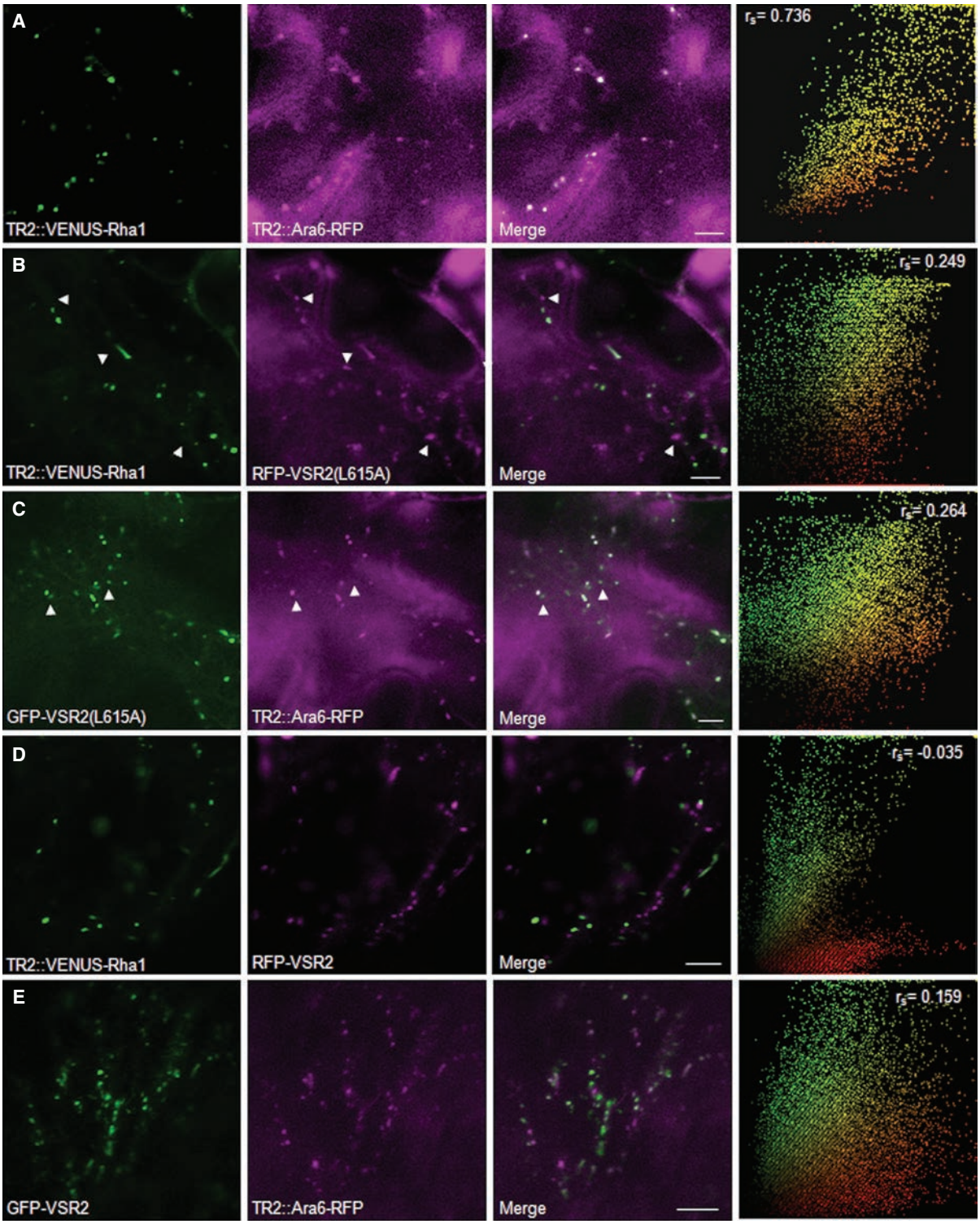

Figure 2: TR2′-driven VENUS-Rha1 and Ara6-RFP label the LPVC. Infiltrated tobacco leaf epidermis cells co-expressing VENUS-Rha1 or Ara6-RFP with each other or individually with either the LPVC marker (VSR2(L615A)) or the PVC marker VSR2 in the appropriate red/green combination. A) VENUS-Rha1 with Ara6-RFP, B) VENUS-Rha1 with RFP-VSR2(L615A), C) GFP-VSR2(L615A) with Ara6-RFP, D) VENUS-Rha1 with RFP-VSR2, E) GFP-VSR2 with Ara6-RFP. White arrow heads in panels B and C indicate VSR2(L615A) in transit through the PVC. At least 300 punctae in a minimum of 10 images were manually masked and analysed with the PSC plugin for ImageJ (24). The resulting scatterplot and the Spearman correlation coefficient (r_s) are shown in the right panel. Notice that the two Rab5 chimera behave differentially only when co-expressed with the PVC marker. Scale bars are 5 μm.

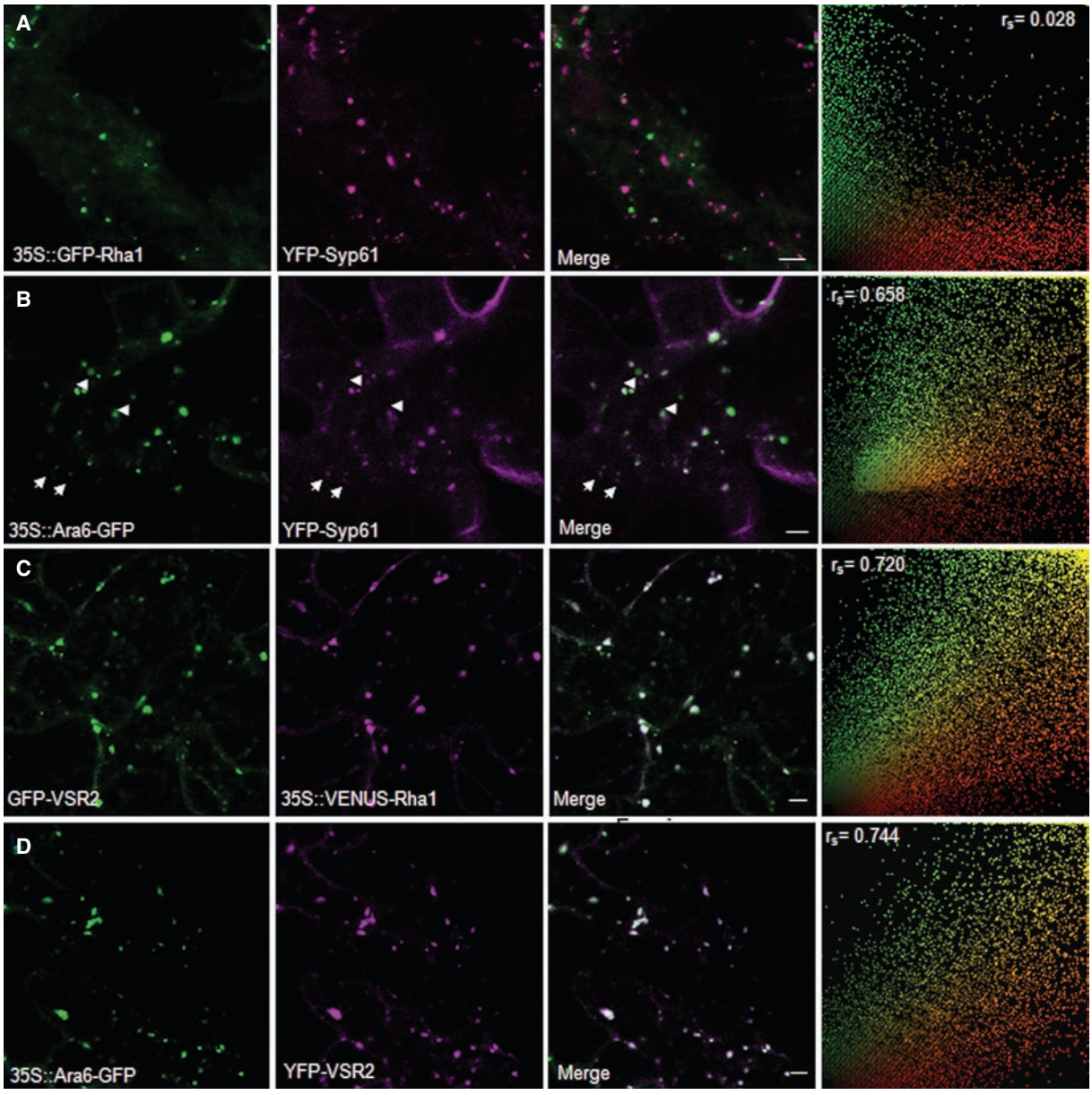

Figure 3: CaMV35S-driven Ara6 and Rha1 cause fusion of post-Golgi organelles. Infiltrated tobacco leaf epidermis cells co-expressing the following combinations of fluorescent protein fusions: A) CaMV35S-driven GFP-Rha1 with the TGN marker YFP-Syp61 (B). CaMV35S-driven Ara6-GFP with YFP-Syp61 (C) GFP-VSR2 with CaMV35S-driven VENUS-Rha1 (D) CaMV35S-driven Ara6-GFP with YFP-VSR2. Notice that under these conditions both Rab5 GTPases co-localized equally well with the PVC marker but can be differentiated when expressed with the TGN marker. In panel B, white arrows indicate structures only labelled by YFP-Syp61 and white arrow heads indicate structures labelled only with Ara6-GFP. Scale bars are 5 μm.

the CaMV35S promoter resulting in a higher correlation (Figure 3D).

Given the fact that overexpressed Ara6-GFP co-localized to both PVC and TGN markers, it was important to test co-expression with a Golgi marker. For this reason, both TR2'- and CaMV35S-promoter fusions for the two fluorescent Rab5 GTPases were co-expressed with the Golgi marker ST-YFP. Figure S3 shows that regardless of expression levels, none of the Rab5 GTPases co-localized with the Golgi marker. This suggests that mistargeting or organelle fusion caused by Rab5 overexpression is restricted to post-Golgi organelles.

In conclusion, overexpression of both Rab5 GTPases causes localization defects but the plant-specific Ara6 shows a higher sensitivity which has a knock on effect on the earlier TGN. Under all circumstances,

the Golgi apparatus remained a completely separate structure.

Rab5 overexpression causes mild secretion of vacuolar cargo

To expand upon the microscopy data, we used a biochemical transport assay with the vacuolar cargo α-amylase-sporamin (amy-spo). This consists of the barley α-amylase reporter fused to the sequence-specific vacuolar sorting signal of sweet potato sporamin (2,3,25). To quantify the effect of various GTPases, a dual expression vector was constructed to contain the Golgi marker ST-YFP (26) under control of the TR2′ promoter as internal standard for plasmid transfection efficiency, routinely tested by western blot (12). The second gene was CaMV35S-driven and included the untagged Rab5 GTPases Rha1, Ara6 as well as the tonoplast localized Rab7 (13). The latter was added as a control because its localization suggests that it may act downstream to the Rab5 family members.

After normalizing the transfection efficiency of the three dual expression plasmids using the internal standard, tobacco protoplasts were co-transfected with constant amounts of amy-spo encoding-plasmid together with dilution series of plasmids encoding for either Rha1wt, Ara6wt and Rab7wt. After 24 h, cells and medium were harvested and the α-amylase activity was quantified in both fractions to determine the Secretion Index (SI = ratio extracellular/intracellular).

Figure 4A shows that increasing concentrations of Rha1wt caused a dose-dependent increase in the SI of the vacuolar cargo which reached ∼3.5× the basal level when the highest concentration of effector was applied. In an almost identical way, overexpression of the plant-specific Rab5 member Ara6wt induced the secretion of amy-spo. In contrast, no increase in the SI was observed upon Rab7wt overexpression. Figure 4B shows that increased SI is not caused by cell mortality because the total activities (TAs) are not reduced by effector co-expression. On the contrary, the reporter seems to be more stable, suggesting that vacuolar sorting and associated protein turnover is inhibited.

As positive control for vacuolar sorting inhibition, we used nucleotide binding mutants of all three GTPases containing an amino acid substitution of the conserved asparagine (N) in the nucleotide binding domain by isoleucine (I). These NI mutants are thought to titrate the guanine nucleotide exchange factor (GEF) involved (27–30) and lead to induced secretion of vacuolar cargo in plant protoplasts (12).

Figure 5A shows that the three mutant GTPases caused a much stronger induced secretion of vacuolar cargo under the same experimental conditions as in Figure 4. Even at the lowest effector plasmid concentration (3 μg), amy-spo secretion was higher than in the case of the

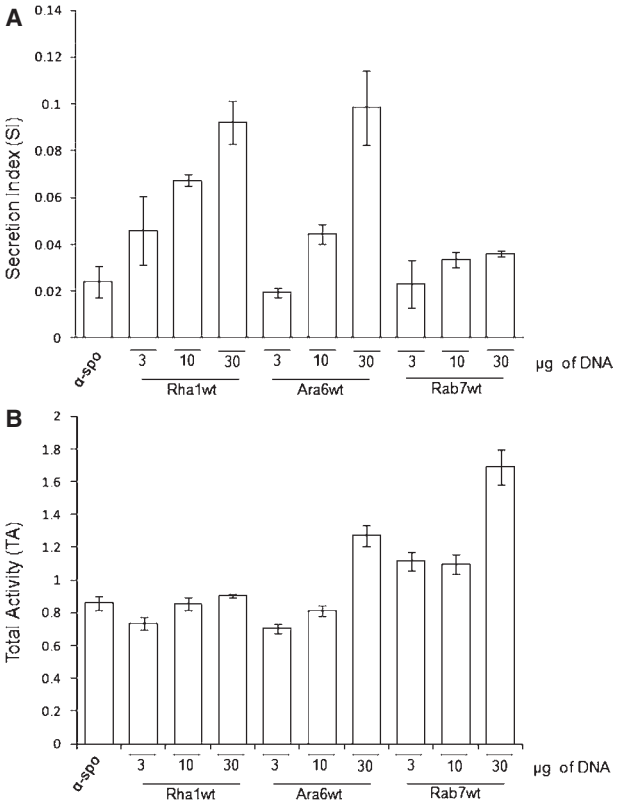

Figure 4: Ectopic expression of wild-type Rab5s lead to mild secretion of the vacuolar cargo amy-spo. A) Tobacco protoplasts were co-electroporated with a constant amount (15 μg) of amy-spo encoding-plasmid with either wild-type Rha1 (Rha1wt), Ara6 (Ara6wt) and Rab7 (Rab7wt) at concentrations in μg indicated in each lane. While Rha1wt and Ara6wt cause a mild but reproducible induction of the secretion of amy-spo, Rab7wt does not interfere with trafficking of the cargo model to the vacuole (B). Total activities (TA = sum of intracellular and extracellular activities) corresponding to panel A. Notice that TAs are not reduced by increased dosage of wild-type Rabs

highest dosage of wild-type Rab5 (30 μg, cf. Figure 5A with Figure 4A). The most striking difference was seen between the effect of Rab7(NI) and Rab7wt, the latter of which showed no effect on vacuolar sorting.

Together with the localization data (Figures 2 and 3), the results suggest that ectopic expression of wild-type Rab5 GTPases inhibits vacuolar sorting and the effects on organelle maturation differentiates between Rha1 and Ara6. In contrast, Rab7 expression levels are not critical for vacuolar sorting.

Differential organelle maturation defects caused by Rha1(NI), Ara6(NI) and Rab7(NI)

We have recently shown that expression of NI mutants of Rha1, Ara6 and Rab7 not only causes induced secretion of soluble vacuolar cargo but also drastic accumulation of cargo in post-Golgi organelles (12). We now wanted to test the effect of the inhibitors on the transport of the

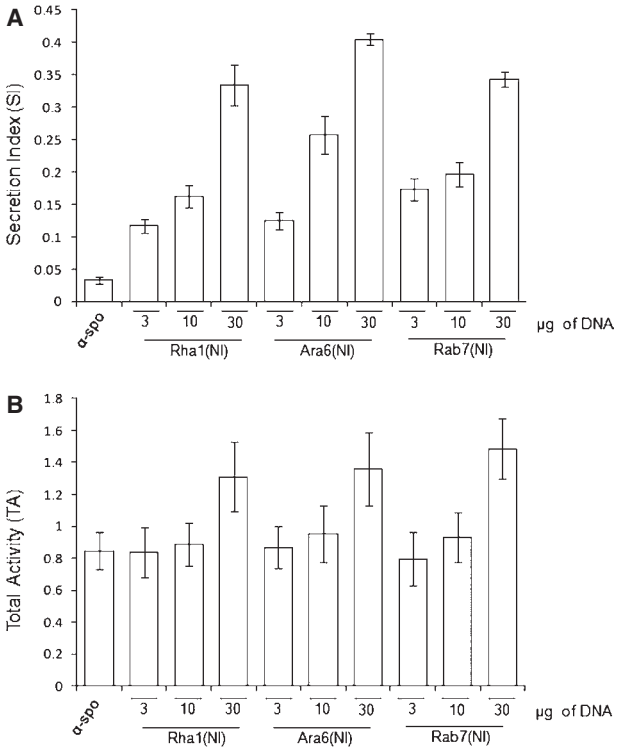

Figure 5: NI mutants of Rha1, Ara6 and Rab7 cause a strong inhibition of amy-spo trafficking to the vacuole. A) Transient expression experiment as in Figure 3 but using nucleotide-free NI mutants of Rha1 (Rha1(NI)), Ara6 (Ara6(NI)) and Rab7 (Rab7(NI)). All other annotations are as in Figure 4. Notice that all the Rab mutants cause a strong dose-dependent secretion of amy-spo into the culture medium. B) Total activities (TA) corresponding to panel A.

VSR responsible for the transport of amy-spo. For this purpose, we compared a wild-type receptor fusion (GFP-VSR2) labelling the PVC with a recycling-defective receptor mutant (RFP-VSR2(L615A)) earlier shown to partition to the LPVC followed by degradation in the vacuole (7).

To guarantee co-expression of the untagged NI mutants with fluorescent PVC and LPVC organelle markers, dual expression vectors for Agrobacterium-mediated plant transformation were generated. The genes encoding the untagged Rab mutants were controlled by the CaMV35S promoter and inserted together with the TR2′-driven LPVC marker RFP-VSR2(L615A) on the same T-DNA. As mock effector, the cytosolic protein Phosphinotrycin acetyl transferase (PAT) was used.

To study PVC–LPVC partitioning, Agrobacterium strains harbouring these dual expression vectors were co-infiltrated in leaf epidermal cells with a strain harbouring the PVC marker GFP-VSR2 encoding-plasmid. Cells exhibiting green and red fluorescence therefore express the green PVC marker, the red LPVC marker as well as the invisible effectors.

RFP-VSR2(L615A) is a recycling-defective receptor that is transported from the LPVC to the vacuole and degraded. In contrast, GFP-VSR2 recycles normally from the PVC and avoids rapid turnover (7). Inhibition of vacuolar delivery is thus expected to specifically increase red fluorescence in PVC/LPVC compartments. In addition, the partitioning between wild-type VSR and recycling-defective VSR may be affected and possibly permit differentiation between the effects of Rha1(NI), Ara6(NI) and Rab7(NI).

The confluent nature of the PVC and LPVC compartments postulated to emerge from continuous retrieval of receptors but not cargo (7) makes it difficult if not impossible to visualize subtle changes with the help of single images. To quantify any changes, a large dataset was required for statistical analysis and calculation of the red/green ratio from scatterplots including all signals. In addition, fluorescent signals were further separated in 16 distinct bins of gradually increasing red-green ratios, followed by normalization of the total green signal across all datasets to permit appreciation of changes in the distribution and strength of the red signal.

Figure 6A shows a representative merged image of at least 20 distinct images from a series of different infiltrations, the sum of which is shown in the scatterplots (Figure 6B) and the population distribution analysis (Figure 6C). In the presence of the mock effector PAT, GFP-VSR2 and RFP-VSR2(L615A) show partial overlap but essentially partition into two separate sub-populations of predominantly green (GFP-VSR2) or predominantly red (RFP-VSR2(L615A)) pixels. This is illustrated much clearer in the distribution analysis which shows, for each category, the proportion of green and red as well as the total sum (grey bars) of fluorescent signals (Figure 6C). This suggests that PVC and LPVC are separate entities as expected under control conditions (7). A red/green ratio of 1.029 (Figure 6B, PAT) shows that the fluorescence of the PVC marker GFP-VSR2 is comparable to the fluorescence of the LPVC marker RFP-VSR2(L615A) and was used as baseline.

In the presence of Rha1(NI), a higher co-localization of PVC and LPVC markers was observed and the red/green ratio was also increased (1.192) compared to the mock effector experiment. Notice the total fluorescence signal (grey bars) in the population analysis displays a single peak.

Ara6(NI) causes a further increase in the red/green ratio (1.224) but in contrast to Rha1(NI), two clear populations remain visible in the scatterplot and in the population analysis. Both the scatterplot and the population analysis are more comparable to the mock effector PAT than Rha1(NI), except for a more prominent red-only population.

Nucleotide-free Rab7 causes the strongest increase of red/green ratio (1.355). In this case, again, two distinct populations of pixel clouds remain distinguishable as in the case of Ara6(NI) or PAT.

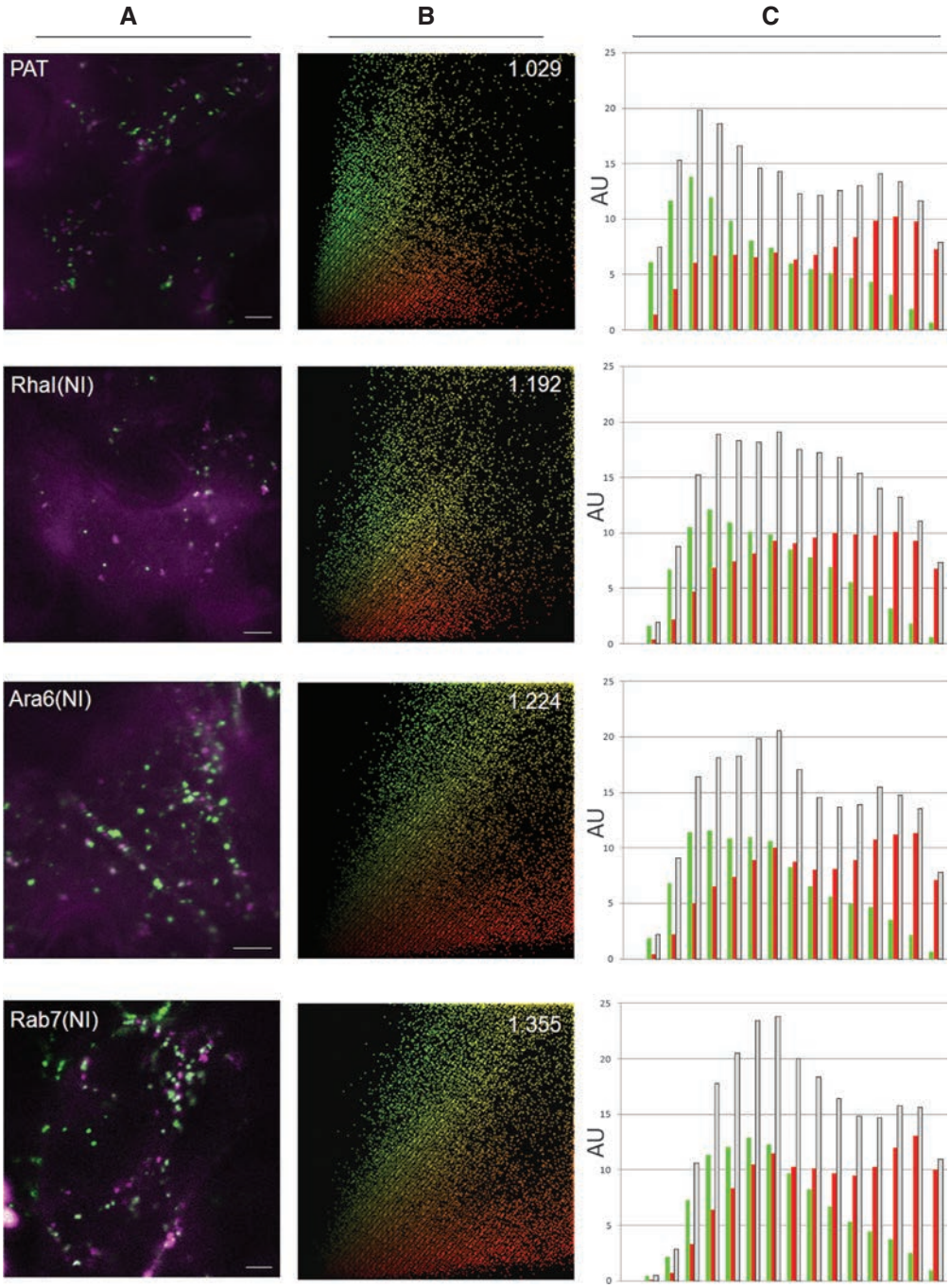

Figure 6: The effect of Rha1(NI), Ara6(NI) and Rab7(NI) on vacuolar delivery and PVC to LPVC maturation. Infiltrated tobacco leaves expressing the PVC marker GFP-VSR2 together with dual expression vectors for the simultaneous expression of the LPVC resident RFP-VSR2(L615A) with either PAT, Rha1(NI), Ara6(NI) or Rab7(NI). The first column (A) shows a representative merged image of the large dataset used to generate the scatterplot (B) from all four co-expression experiments. Scatterplots were generated as described in Figure 2. The total green and red fluorescence in the scatterplots was quantified and the red/green ratio is indicated in the top right corner of the scatter plots. The third column (C) shows a population analysis of the whole dataset. The fluorescent pixels obtained were grouped into 16 different categories with increasing red/green ratios. The first bin indicates all pixels that have a red/green ratio between 0 and 6.25% red, the second bin includes ratios from 6.25 to 12.5% red and so on until the 16th and final bin which includes 93.75–100% red. Notice that the first bin is empty in all cases. The sum of all green signals for each of the four datasets has been normalized to 100%. Individual bins show the total green, red and sum (grey bars). Notice that the population profile for the Rha1(NI) experiment deviates from that of the other three, showing a single peak as opposed to two distinct peaks.

Figure 3 showed that wild-type Ara6 could potentially cause TGN-PVC fusion or protein mistargeting between these two compartments. To test this possibility for the dominant-negative NI mutants, the four dual expression vectors were re-constructed to replace the TR2'-driven LPVC marker RFP-VSR2(L615A) by the TGN marker YFP-Syp61. These were co-transformed with an Agrobacterium strain harbouring the PVC marker GFP-VSR2. In all four cases, there was no overlap between the TGN and PVC markers (Figure S4). The results indicate that organelle maturation defects caused by wild-type Rab5 overproduction are clearly distinct from those observed with the NI mutants.

Taken together, the data suggest that NI mutants of Rha1, Ara6 and Rab7 cause increased retention of recycling-defective RFP-VSR2(L615A) in the PVC as visible by a yellow shifted green population of pixels. The tendency for this effect increases from Rha1(NI)<Ara6(NI)<Rab7(NI). However, only Rha1(NI) appeared to cause a distinct partitioning defect leading to merging of PVC and LPVC markers. It should be noted that these differences can only be noticed from a statistical analysis of a large data set, none of which would be noticeable from single images (Figure 6A).

In conclusion, a difference between the canonical and plant-specific Rab5 GTPases continues to be apparent as earlier observed in Figures 2 and 3 and previously published findings (20,31). Moreover, the defect caused by nucleotide-free Rab7 can be mapped later than Rab5(NI) action as suggested by the more prominent red fluorescent LPVC accumulation in comparison to the other inhibitors.

Ara6(NI) titrates the putative Rab5 GEF Vps9

Previous studies have indicated functional differences between canonical and plant unique Rab5 GTPases (20). Vps9 was shown to act as GEF for both classes of plant Rab5 GTPases *in vitro*, yet only the canonical C-terminally lipid anchored Rab5GTPase can suppress a Vps9 knock-down phenotype on root elongation when expressed as GTP-locked permanently activated form. The plant Rab7 GEF is currently unknown and either the monomeric VPS39/Vam6 or the dimeric Mon1-Ccz1 complex have been proposed as GEFs for YPT7 in yeast (32,33). We have chosen the monomeric Vam6 as test object for our transient expression experiments as the Arabidopsis homologue was readily identified from the databases in contrast to Mon1 and Ccz1.

We now wanted to test if the inhibitory effect of NI mutants of Rab GTPases can be explained by titration of the specific GEF using either the plant VPS9 or plant VPS39/Vam6 as test objects. If a GEF becomes the limiting factor in a transport reaction (27), reintroduction of further GEF molecules should restore sorting. In addition, overexpression of the GEF itself can cause titration of its substrate GTPase, as specifically shown for the GTPase Sar1 and its exchange factor Sec12 (34).

Figure 7A shows that neither overexpressed Vps9 nor Vps39/Vam6 caused vacuolar sorting defects as seen by no significant increase in amy-spo secretion. This suggests that the two GEFs do not titrate any critical factor when expressed alone, possibly because the GTPases are present in excess and are not limiting.

To test if either of the GEFs are limiting when plant Rab5 NI mutants are expressed, increasing concentrations of a plasmid harbouring either Vps9 or Vam6 overexpression constructs were added to constant levels of cargo and inhibitors. Figure 7B shows that Vps9 reduced Ara6(NI)-induced amy-spo secretion in a dose-dependent manner, suggesting that it is one of the limiting factors when Ara6(NI) is expressed. In contrast, VPS39/Vam6 fails to restore correct sorting as the SI remains unchanged (Figure 7C). This illustrates the specificity of Vps9 in its ability to suppress Ara6(NI)-induced amy-spo secretion. Interestingly, Vps9 had no effect on Rha1(NI)-induced amy-spo secretion (Figure 7D). On the contrary, a small but reproducible aggravation of Rha1(NI)-induced amy-spo secretion was observed.

Although Vps9 was reported to act as GEF on all the Rab5 members *in vitro* (20), the situation appears to be more complex *in vivo* where Vps9 does not seem to be the limiting factor when Rha1(NI) is expressed. The results support the idea that Rha1 and Ara6 may be functionally different.

Evidence for functional differentiation of the Rab5 family members in plants

Although NI mutants are expected to titrate the GEF involved, this may not be true for all GTPases. Indeed, plant wild-type GTPases Rab1 and Ara7 were reported to be able to complement their nucleotide-free and GDP-trapped mutants respectively (11,35). To test this, we repeated the experiment in Figure 7B and D but using the wild-type Rabs as suppressors.

Figure 8A shows that wild-type Ara6 is not able to effectively restore vacuolar sorting in the presence of its dominant-negative mutant. However, it is interesting to note that it does not aggravate the effect as could be implied from the fact that wild-type Ara6 overdose induces secretion of amy-spo as well (Figure 4). The same dose-response experiment was carried out for the canonical Rab5 family member Rha1 (Figure 8B). In contrast to Ara6, wild-type Rha1 strongly suppressed the effect of its nucleotide-deficient mutant. This was unexpected because Rha1 wt overexpression alone interferes with vacuolar trafficking as much as Ara6 (Figure 4A).

To test these differences further, a reciprocal suppression experiment was performed. Figure 8C shows that

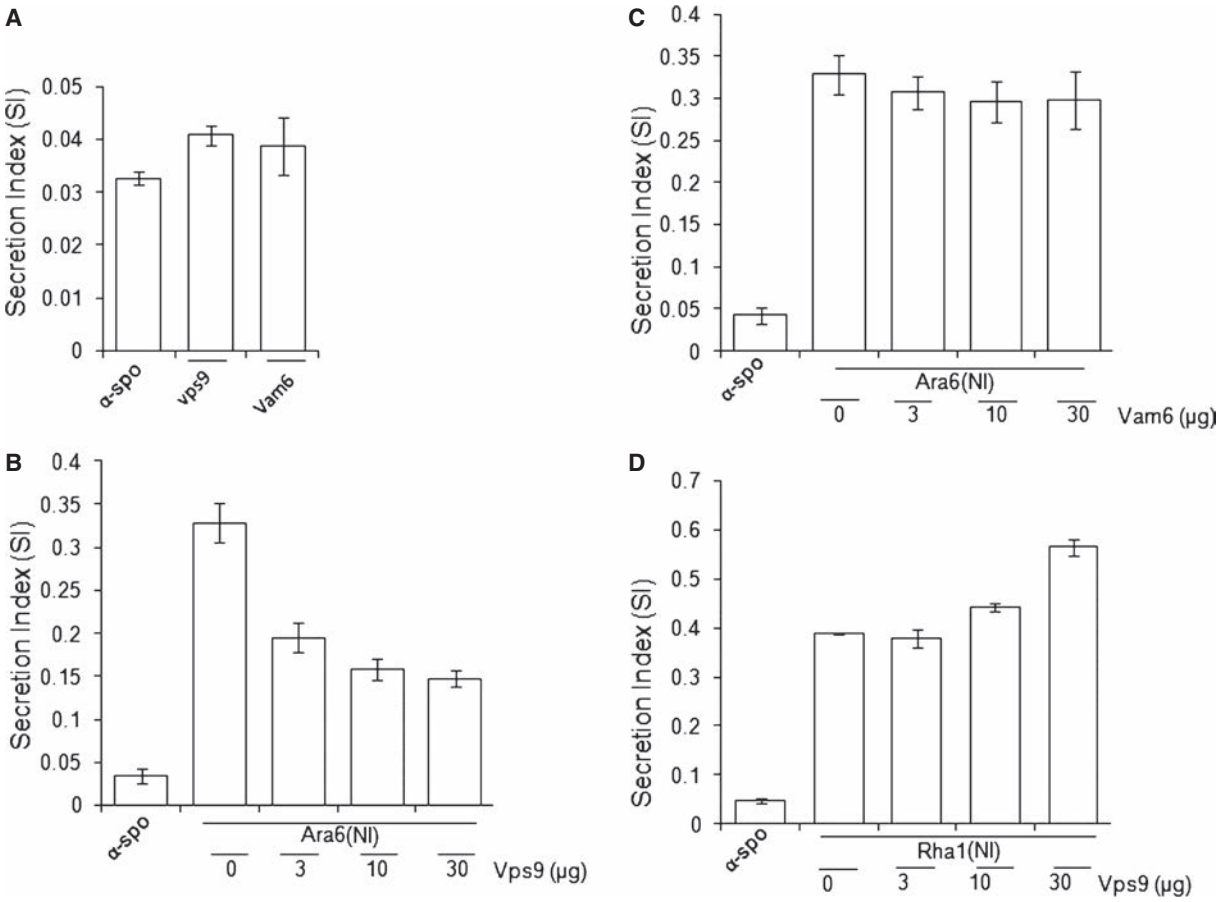

Figure 7: Differential rescue of vacuolar sorting by the Rab5 GEF Vps9 suggests functional differentiation between Rha1 and Ara6. A) Tobacco protoplasts co-electroporated with constant amounts (15 μg) of amy-spo encoding-plasmid alone or together with plasmids encoding either Vam6 or Vps9 (30 μg). The two putative GEFs do not induce noticeable secretion of the vacuolar marker amy-spo. Tobacco protoplasts co-electroporated with constant amounts (15 μg) of amy-spo encoding-plasmid, together with constant amounts (30 μg) of either Ara6(NI) (B, C) or Rha1(NI) (D) to inhibit vacuolar sorting and increasing concentrations of either vps9 encoding-plasmid (B, D) or Vam6 encoding-plasmid (C) at quantities indicated in each lane in μg. Notice that Ara6(NI)-induced secretion of amy-spo could only be suppressed by increasing doses of Vps9.

increased dosage of wild-type Ara6 had only a minor effect on Rha1(NI) induced amy-spo secretion. In sharp contrast, wild-type Rha1 strongly suppressed Ara6(NI)-induced amy-spo secretion (Figure 8D).

Together, the results suggest that the GTPases Rha1 and Ara6 exhibit different properties regarding the mechanism by which nucleotide-free mutants inhibit vacuolar sorting. NI mutants of both Rab5 members cause Rha1 to be limiting, but only Ara6(NI) can be suppressed by its GEF Vps9.

Rab7(NI) is truly dominant negative

In contrast to the Rab5 members analysed, Rab7 only inhibited vacuolar sorting as (NI) mutant (Figure 5) but not when overexpressed as wild type (Figure 4). To identify limiting factors, suppression was tested with wild-type Rab7 as well as the two GEFs, Vps9 and Vam6. Figure 9 shows that none of the candidates could suppress Rab7(NI)-induced amy-spo secretion, including the putative Rab7 GEF Vam6 (Figure 9B).

In conclusion, it is not clear at this stage which factor is limiting when vacuolar sorting is disrupted with nucleotide-deficient Rab7. In contrast, nucleotide-deficient Rab5 members either titrate the exchange factor Vps9 or the wild-type form of the GTPase itself.

Discussion

Rab5 and Rab7 GTPases are markers for the late prevacuole and vacuolar membrane respectively in tobacco leaf epidermal cells

We have recently shown that plant PVCs fall into two categories, an early PVC that exhibits a high steady-state level of VSRs and a 'late' PVC (LPVC) that is enriched in soluble vacuolar cargo and depleted in VSRs (7).

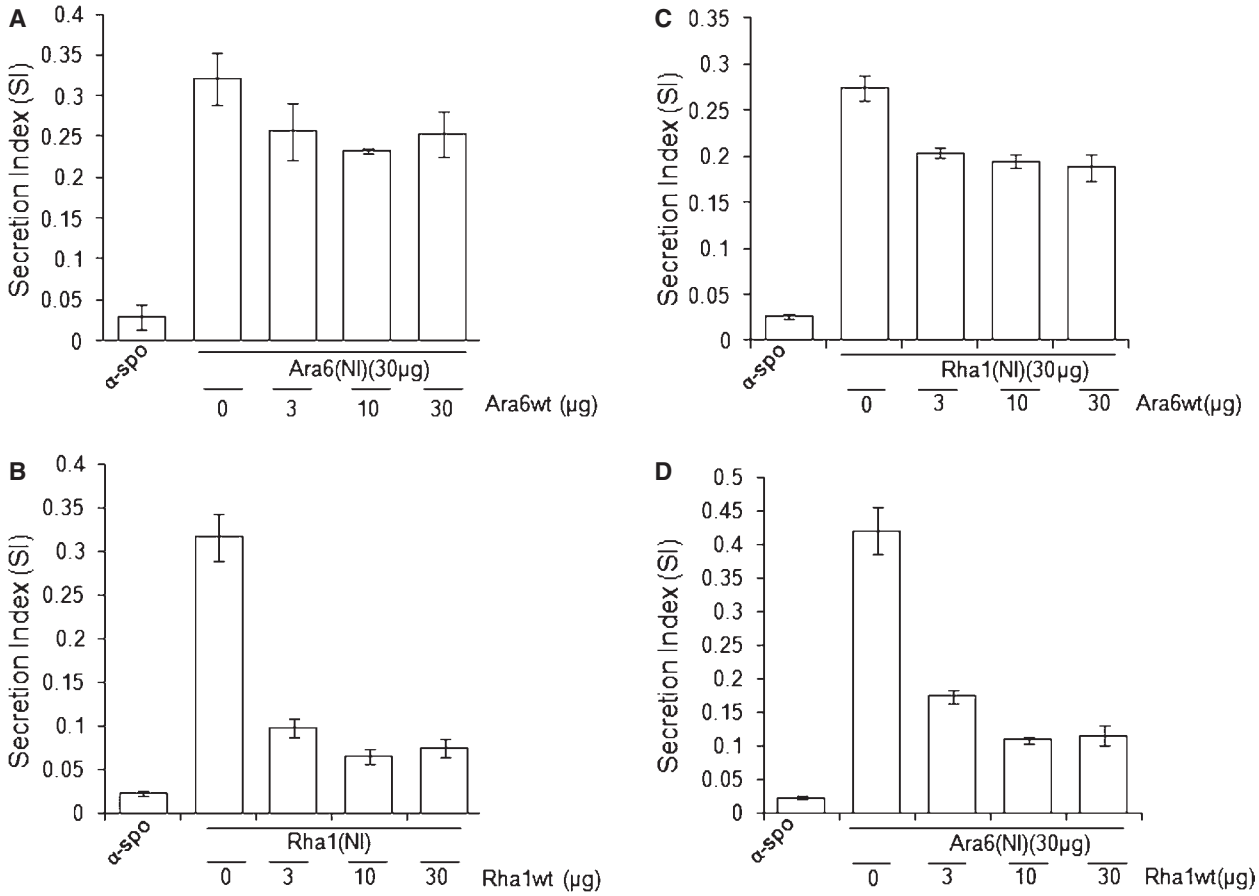

Figure 8: Rha1(NI)- and Ara6(NI)-induced secretion of vacuolar cargo can both be suppressed by wild-type Rha1. Tobacco protoplasts were co-electroporated with constant amounts (15 µg) of amy-spo encoding-plasmid together with constant amounts (30 µg) of either Ara6(NI) (A,D) or Rha1(NI) (B,C) as vacuolar sorting inhibitors, supplemented by increasing amounts (indicated in each lane) of either Ara6wt or Rha1wt. Notice that increasing concentrations of Rha1wt could suppress the inhibitory effect on vacuolar sorting of both Rab5 classes mutants (B,D).

Interestingly, a representative of the canonical Rab5 GTPases Rha1 also labels this novel compartment. Here, we show that both canonical and plant-specific Rab5 members co-localize predominantly with an LPVC marker when they are expressed from a weak promoter in leaf epidermis cells (Figure 2). Moreover, PSC correlation analysis from large data sets did not reveal evidence for differential localization of the two classes of Rab5 GTPases in relation to each other, in contrast to previous reports (18,19). The results are in agreement with the reported localization of all Rab5 members in multivesicular bodies (21).

We also show that the Arabidopsis Rab7 homologue labels the tonoplast of tobacco leaf epidermal cells when expressed at low levels. We noticed that Rab7 has a higher tendency to label the cytosol compared to the two Rab5 GTPases and low expression is essential to visualize Rab7 on the vacuolar membrane. It is possible that post-translational modification of the Rab7 C-terminus to acquire the lipid anchor is slower than that of Rab5 members, it also possible that steady-state levels of Rab7 are shifted towards the inactive GDP-bound form whereas Rab5 members readily partition to LPVC membranes, even when expressed by the strong CaMV35S promoter. Further work is needed to test these possibilities.

Compared to previously reported subcellular localization data on Rab7 (13,14), we notice similarities as well as differences that could reflect specialization in species and tissues. Rab7 not only decorated the delimiting vacuolar membrane of tobacco leaf epidermis cells but also the intravacuolar 'bulbs' (Figure 1A), in contrast to earlier findings (13). However, we have noticed that bulb formation is a highly variable phenomenon and we see variations from cell to cell, within the same tissue. In *Medicago truncatula* roots and root hairs, Rab7 was found at the tonoplast as well as on punctate structures (14). We could not detect such structures in tobacco leaf epidermal cells under the experimental conditions used. This could either be due to the species, cell type or the experimental procedures.

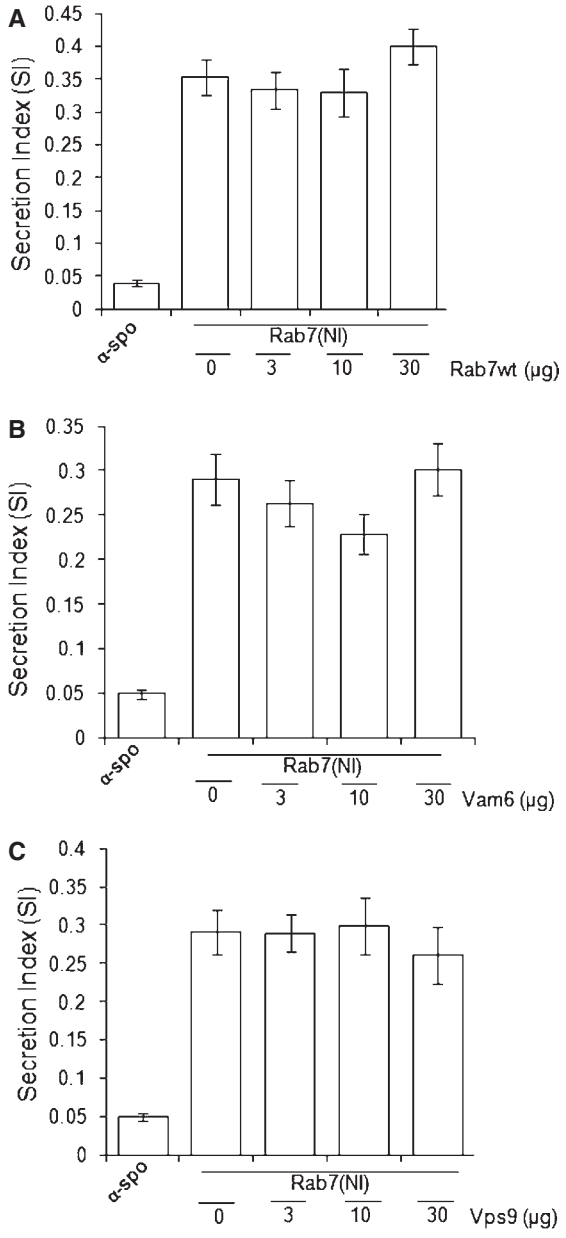

Figure 9: Nucleotide-free Rab7 is truly dominant-negative. Suppression of nucleotide-free Rab7 action was attempted with Rab7wt (A), Vam6 (B) and Vps9 (C). All annotations are as in Figure 7. No reduction of the SI was observed in any of the cases.

Rab GTPases recruit a wide variety of effectors to regulate processes such as vesicle budding, uncoating, tethering to membranes and the cytoskeleton as well as modifications in the lipid composition (36). It is interesting to note that the Rab1 GTPases control ER to Golgi traffic (35) and show highest steady-state levels at the target organelle, the Golgi apparatus (37). Unlike mammalian Rab5 GTPases, the plant counterparts label the late prevacuoles. This also corresponds with the fact that Rab7 GTPases accumulate at the mammalian late endosomes while in plants they label the tonoplast.

Overexpression of wild-type Rab5 GTPases influences vacuolar sorting

The results presented here show that even mild overexpression of wild-type Rab5 GTPases can cause post-Golgi organelle fusion (Figure 3) as well as vacuolar transport defects (Figure 4). This effect is more pronounced for the plant-specific form Ara6 and first appears to result in PVC–LPVC fusion at modest TR2′-promoter driven ectopic expression (Figure 2E). At higher expression levels, wild-type ARA6 seems to cause the formation of a TGN–PVC–LPVC super-compartment (Figure 3B–D), not unlike wortmannin-induced TGN–PVC fusions reported earlier (38). In contrast, Rha1 overexpression resulted in PVC–LPVC fusions only when the strong CaMV35S promoter was used (Figure 3C). The difference in sensitivity to expression levels may explain some of the earlier results suggesting that Rha1/Ara7 label different endosomes compared to the plant unique Ara6 (18,19).

The implementation of a quantitative cargo transport assay using double expression vectors for controlled dose–response assays provided convincing evidence showing that the ectopic expression of wild-type Rab5 family members Rha1 and Ara6 leads to missorting of vacuolar cargo (Figure 3A). This is not an unspecific effect because overexpression of a plant tonoplast Rab7 GTPase had no effect on vacuolar sorting when overexpressed as wild type.

Although numerous reports illustrated Rab5 mediated inhibition of vacuolar sorting upon expression of dominant-negative mutants (9–11), it is novel that overdose of wild-type GTPases could have an inhibitory effect as well. This is even more astonishing in the light of past reports proposing that wild-type Rab5 overexpression can restore proper vacuolar targeting in the presence of GDP-trapped Rab5 mutants (11). Typically, overexpression effects are due to titration of other interacting factors (34) which can shed light on protein–protein interactions involved. Hence, it would be interesting to identify limiting factors when Rab5 GTPases are ectopically expressed.

Nucleotide-free (NI) mutants of Rha1 but not Ara6 affects VSR partitioning between the PVC and the LPVC

Quantitative dose–response assays revealed that nucleotide-free mutants of both Rab5 GTPases exhibit a much stronger inhibition of vacuolar sorting compared to their wild-type forms (cf. Figure 5 with Figure 4). Interestingly, the effect on the post-Golgi organelles is distinct from those of the ectopic expression of the wild-type proteins. Wild-type Ara6 overexpression caused co-localization of TGN and PVC markers (Figure 3B). Expression of the corresponding NI mutant did not

alter the partitioning between these two organelles (Figure S4). Wild-type Rha1 does not affect TGN–PVC marker partitioning, whereas NI mutant causes defective partitioning between PVC and LPVC markers (Figure 6). The overall response pattern of the Rab5(NI) mutants is therefore very different from those observed with the wild-type proteins.

When comparing the three different NI mutants, Rha1 seems to have a slightly different affect when compared to the other mutant proteins (Figure 6). This is best illustrated by the population analysis (Figure 6C). However, it must be appreciated that microscopy analysis alone cannot provide further insight into the biochemical differences between the two classes of Rab5 GTPases.

Vps9 is the exchange factor for the plant-specific Rab5 Ara6

The strong knowledge-base gained on the Ras GTPases has provided the field with tools to generate mutants, the best characterized of which can be classified into GDP-locked (SN), GTP-locked (QL) or nucleotide-free (NI) varieties (39). Depending on the type of GTPase and the transport step they control, these mutants often display dominant-negative effects that can interfere with the endogenous wild-type genes. However, there is no common principle to predict inhibitory functions due to the wide variety of Rab-effector interactions.

GEFs exhibit a conformational switch to display a high affinity to catalytically inactive GDP-bound GTPases and a low affinity to the activated GTP-bound state of the GTPase (30). It was generally assumed that the GDP-locked mutant GTPases impose their inhibitory effect by titration of their associated GEF, an effect that would be dominant because wild-type Rab would no longer be activated. Similarly, the NI substitution in the GTPase nucleotide binding domain has also been suggested to lead to titration of the GEF involved (27,29).

Here, we have tested the premise that NI mutants of GTPases titrate the GEF involved (27) and attempted to restore vacuolar sorting by gradually increasing Vps9 expression levels. Overexpressed Vps9 can clearly suppress the inhibitory effect on vacuolar sorting caused by Ara6(NI) but not Rha1(NI) and Rab7(NI) (Figure 7). The results indicate that Ara6(NI) disrupts vacuolar sorting by titrating Vps9 until it becomes limiting. However, in cells expressing Rha1(NI), the limiting factor cannot be Vps9 because its overexpression cannot restore vacuolar sorting.

Consistent with these observations, overexpression of wild-type Ara6 could not suppress the Ara6(NI) phenotype (Figure 8A) in contrast to earlier observations on the canonical Rab5 form Ara7 (11). However, vacuolar sorting defects induced by Rha1(NI) were strongly suppressed by increasing Rha1 wild-type levels (Figure 8B). The latter is remarkable because wild-type Rha1 causes mild vacuolar sorting defects when overexpressed alone (Figure 4). Even more remarkable is the fact that wild-type Rha1 can also suppress the Ara6(NI) mediated vacuolar sorting defect (Figure 8D).

Together, these results are certainly in strong agreement with earlier observations regarding functional differentiation between the plant-specific Ara6 and the other two canonical Rab5 GTPases (18–20). Mammalian Rab5 has been implicated in various cellular processes from endocytosis to early endosome homotypic fusion (36). Functional differentiation is thought to arise from the interaction with different GEFs and effectors. Rme-6 is involved in formation of clathrin coated pits at the PM (40,41) while Rabex-5 is implicated in fusion of early endosomes (42). The scenario may be similar in plants with Rha1/Ara7 performing a different function and therefore interacting with a different set of effector proteins compared to Ara6. Alternatively, Ara6 may act earlier and activate a Rha1-dependent pathway. This could become partially redundant upon Rha1 overexpression. Finally, it cannot be ruled out that the two classes of Rabs simply exhibit differential nucleotide affinities. If Rha1 does not require Vps9 for nucleotide exchange, then it would not be limiting when Rha1(NI) is expressed. On the other hand, Rha1(NI) overexpression may titrate a component that is also needed for Ara6 functioning. Therefore, overexpression of Ara6wt would not alleviate Rha1(NI). In conclusion, it is not clear whether Rha1 and Ara6 are biochemically different (they do not share the same effector molecules) or the differentiation is in the trafficking steps catalyzed.

Dominant-negative nature of the tonoplast GTPase Rab7

While it was shown that upon overexpression of Rha1(NI) and Ara6(NI) the limiting factors can be the GTPase itself (Figure 7B) or the GEF Vps9 (Figure 6B) respectively, the tonoplast localized Rab7 seems to behave in a completely different way compared to the Rab5 group. Neither the wild-type form of Rab7 nor the putative Rab7 GEF Vam6 suppress Rab7(NI) mediated vacuolar sorting defects (Figure 9A, B). This suggests that suggesting that Vam6 is either not the Rab7 GEF or that Rab7(NI) may titrate some other unknown component.

Vam6 has been shown to bind to the GDP-bound form of Ypt7 in yeast and promote nucleotide exchange (32). However, recently the mammalian homologue failed to promote GTP binding of Rab7 and the authors suggested that another as yet unidentified protein may perform the role of Rab7 GEF in mammals (43). The recently described dimeric Mon1-Ccz1 complex (33) could be a good candidate. Further work will have to be done to identify the true Rab7 GEF in plants.

Current working model

The results obtained in this study illustrate clear differences between the two classes of Rab5 GTPases

and Rab7. Although many alternative explanations can be explored, we would like to present a working model that can help to explain the current data (Figure 10). At low expression, both Rab5 forms are localized to the LPVC while Rab7 is found on the vacuolar membrane. In addition, functional differences between the two Rab5 GTPases were established via suppression experiments with VPS9 as well as wild-type Rha1.

Although both GTPases occupy the same organelle when expressed at low non-perturbing levels, they appear to control vacuolar sorting in different manners. Microscopy provides indications regarding the potential position in the pathway at which they exhibit control. Overexpression of wild-type Ara6 causes sorting defects that include the earlier TGN marker. Since expression is a variable largely dependent on the model system used, the results may explain some of the conflicting reports in the field. In particular, the Ara6-induced co-localization of TGN and LPVC markers resemble those induced by the drug wortmannin. Ara6 could control recycling of SNAREs and receptors from the PVC (1) and may indirectly also be required for anterograde transport. The recent suggestion that Ara6, but not Rha1/Ara7, play a role in transport to the plasma membrane corresponds with this model (19).

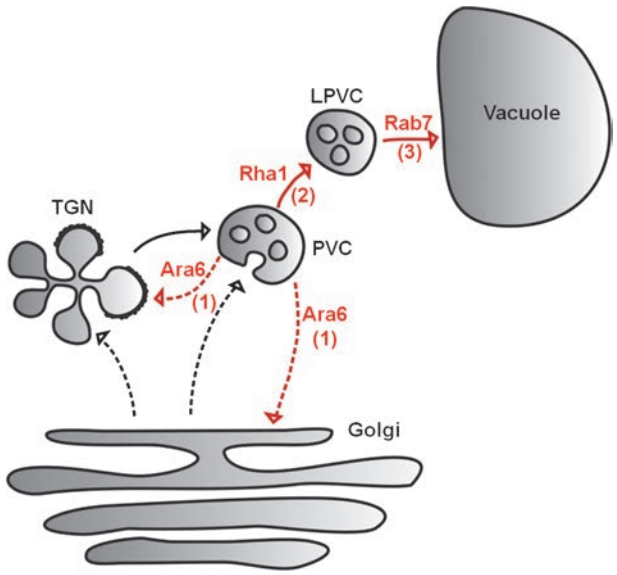

Figure 10: Proposed model for the functioning of Rab5s and Rab7 in the late secretory pathway. Simplified schematic showing the Golgi apparatus and post-Golgi organelles thought to be involved in vacuolar transport. *Trans*-Golgi network (TGN), prevacuolar compartment (PVC), late prevacuolar compartment (LPVC). Transport routes indicated by dashed arrows represent hypothetical pathways that have yet to be established. The plant-specific Ara6 may play a role in recycling of VSRs and other machinery components from the PVC to earlier compartments (1). Rha1 may be involved in the actual PVC to LPVC maturation step (2), Finally Rab7 is likely to be part of the machinery responsible for vacuolar delivery (3).

Rha1(NI) appears to disturb a later step in the pathway and could interfere with PVC to LPVC maturation. Although no direct evidence for maturation has been obtained, it was demonstrated that VSRs depend on an active sorting signal to avoid mistargeting to the LPVC and vacuole (7). In the absence of experimental evidence for a vesicle shuttle mediating PVC to LPVC transport, the maturation model by receptor depletion is the simplest and thus preferred model. Rha1/Ara7 may control a later step in PVC maturation (2), because Rha1 manipulation never caused any effects at the level of the TGN, in contrast to Ara6.

Finally, Rab7 probably acts after the two Rab5 GTPases, during the final LPVC to vacuole transport step (3). This is strongly supported by the fact that Rab7(NI) caused retention of the tonoplast marker Vam3 while Rab5(NI) mutants did not (12). In addition, Rab7(NI) did not affect partitioning between PVC and LPVC markers, and showed the strongest LPVC retention of the recycling-defective VSR(L615A) which is normally degraded in the vacuoles. Finally, the localization of Rab7 to the last membrane of the vacuolar route adds further support to the sequential hypothesis.

Further protein components of the PVC and LPVC compartments need to be identified to help understanding PVC dynamics and post-Golgi protein sorting to the plant vacuole.

Materials and Methods

Recombinant DNA plasmids encoding organelle markers molecules

Recombinant plasmids previously described in the literature were used in this article. These include GFP- and RFP-VSR2, GFP- and RFP-VSR2(L615A), RFP-Syp61 (7), YFP-Syp61 (44), ST-YFP (26), ST-CFP (12) and amy-spo (3,25).

Cloning of Rab GTPase coding regions, generation of fluorescent chimeras and mutagenesis

cDNA from 5-day-old seedlings was used as a template for the amplification of Rab GTPases coding sequences (25). The Rab5 members Rha1 and Ara6 as well as Rab7 coding regions were amplified to yield *Nco*I–*Xba*I flanked coding regions with sense and antisense primers indicated in Figure S5A. After digestion and gel-purification, these were ligated into pAmy-HDEL (45) previously cut with *Nco*I–*Xba*I and dephosphorylated to yield pRha1, pAra6 and pRab7.

CFP-Rab7 under control of either CaMV35S or TR2′-promoters was generated by fusing a ClaI NcoI CFP fragment in frame to the NcoI site of Rab7 and the ClaI site of either promoter in a pUC plasmid.

TR2-driven VENUS-Rha1 was generated as described in (7) pTR2::VENUS-Rha1 was cut with *Cla*I and *Hin*dIII dephosphorylated and used as a vector to generate pTR2::Ara6-RFP. The Ara6 fragment was generated by amplifying pAra6 with an Ara6 sense primer and *Xba*I antisense primer (Figure S5A), cut with *Nco*I and *Xba*I and gel purified. A fragment containing the RFP coding region plus the 3′nos polyadenylation signal fragment was generated by amplifying ST-RFP (7) with an RFP sense and a pUC antisense

primer annealing to the pUC backbone after the 3′nos fragment, cut with *Xba*I and *Hin*dIII and gel purified. The Ara6 and the RFP fragments were then ligated into the previously generated vector to yield pTR2::Ara6-RFP.

The GFP fragment for the generation of CaMV35S::Ara6-GFP was generated by amplifying cytosolic GFP (46) with a GFP sense primer and an antisense primer annealing the pUC plasmid after the end of the 3′nos polyadenylation signal (pUCas), cut with *Nhe*I and *Hin*dIII and gel purified. The Ara6 fragment was generated by amplifying pAra6 with an Ara6 sense and an Ara6 NheI antisense primer, cut with *Nco*I and *Nhe*I and gel purified. The fragments were then ligated into a previously cut with *Nco*I and *Hin*dIII and deposphorylated amy-HDEL plasmid (34).

A VENUS-Rha1 fragment was generated by cutting pTR2::VENUS-Rha1 with *Cla*I and *Nco*I and gel purified. The fragment was then ligated into a previously cut with *Nco*I and *Hin*dIII and deposphorylated amy-HDEL plasmid (34) yielding pCaMV35S::VENUS-Rha1.

A GFP fragment was generated by amplifying cytosolic GFP (46) with a GFP sense and antisense primers, cut with *Cla*I and *Nco*I and gel purified. The fragment was then ligated into a previously cut with *Cla*I and *Nco*I and deposphorylated pCaMV35S::VENUS-Rha1 yielding pCaMV35S::GFP-Rha1.

All the described expression cassettes were excised from pUC vectors as *Eco*RI and *Hin*dIII flanking fragments and cloned into the polylinker of the *A. tumefaciens* transformation vector pDE1001 (47)

Mutagenesis of all Rabs to generate the NI mutants was done via the QuickChange method (Stratagene) using pairs of oligonucleotides encoding for the mutated triplet and 15 bases extending on either side of the mutated codon. All mutagenesis primers for each specific Rab GTPase are shown in Figure S4B. All resulting clones were verified by sequencing.

Dual expression vectors

Several steps were required to generate the dual expression vector using primers described in Figure S4C. A TR2′-promoter fusion with the Golgi marker ST-YFP was generated by assembly PCR using first the primer pair TR2EcoRIs with TRSTYas and the plasmid pOP443 (23) as template, resulting in a modified TR2′-promoter fragment. The primer pair TRSTYs with STYas and plasmid pLL4 (3) as template were used to generate a modified ST-YFP fragment. The two overlapping fragments were subsequently subject to 10 PCR cycles for self-priming, followed by further PCR amplification using the primer pair TR2EcoRIs with STYas to yield the assembled 3′ocs::CaMV35Spromoter fragment. This was trimmed with *Eco*RI and *Xba*I and gel purified.

PCR assembly of the 3′ocs::CaMV35Spromoter fragment was performed with primer pair 3ocsXba1s with 3ocs35Sas and plasmid pDE1001 (47) as template to generate a modified 3′ocs sequence. The primer pair 3ocs35ss with amyas and plasmid pAmy as template (45) resulted in the amplification of a modified CaMV35S promoter fragment. The two overlapping amplification products were subsequently subject to 10 self-priming PCR cycles to generate an assembled fusion, followed by further PCR amplification using the primer pair 3ocsXba1s with amyas to yield the assembled 3′ocs::CaMV35Spromoter fragment. This was ultimately trimmed with *Xba*I and *Nco*I and gel purified.

To generate the double expression vector, plasmid pDE317 was cut with *Eco*RI and *Nco*I to remove the CaMV35S promoter in front of the PAT-3′nos region (47) followed by dephosphorylation. The two assembled and trimmed DNA fragments described above were ligated into this vector to generate plasmid pFB62 carrying the dual expression cassette TR2-ST-YFP-3′ocs/CaMV35S-PAT-3′nos. This plasmid was used as starting point for all subsequent double expression vector constructions.

The PAT coding region in pFB62 was removed with an *Nco*I–*Bam*HI digestions followed by dephosphorylation. All Rab GTPase coding regions and mutations thereof were isolated as compatible *Nco*I-*Bam*HI fragments and ligated into pFB999. These plasmids were used for quantitative transient expression experiments in conjunction with pAMY derivatives. For tobacco leaf infiltrations, the entire double expression cassettes were cloned between the *Eco*RI and *Hin*dIII sites of pDE1001 (47) using standard recombinant DNA procedures, yielding pTFB62 and derivatives containing Rab coding regions.

The Golgi marker ST-YFP was replaced by the TGN marker YFP-Syp61 (44) by cutting pTFB62 with *Eco*RI and *Xba*I and dephosphorylation. pTFB62 was also cut with *Cla*I, followed by Klenow treatment, and subsequent *Eco*RI digestion and gel-purification. The YFP-Syp61 fragment was obtained by cutting pOF61 with *Nco*I, followed by Klenow treatment, subsequent *Xba*I digestion and gel-purification. The two fragments were then jointly ligated into pTFB62, to yield pTFB73 carrying the dual expression cassette TR2-YFPSYP61-3′ocs/CaMV35S-PAT-3′nos. pTFB62 was cut with *Xba*I, *Kle*now, and *Cla*I, followed by dephosphorylation to generate a vector. RFP-VSR2(L615A) was obtained by cutting pOF102 (7) with *Bam*HI, Klenow, ClaI, and gel-purification, for ligation into the vector. This resulted in plasmid pTFB97 carrying the dual expression cassette TR2-VSR2(L615A)-3′ocs/CaMV35S-PAT-3′nos. In all the dual expression vectors, replacement of PAT by the various Rabs was carried out as for pFB62.

Transient expression in tobacco protoplast and α-amylase assay

Nicotiana tabacum cv Petit Havana SR1 (48), were grown in a controlled room at 22°C with a 16-h daylength at a light irradiance of 200 μE m^2 on Murashige and Skoog (MS) medium +2% sucrose (49). Preparation, electroporation and harvesting of protoplasts were carried out as previously described (50). Concentrations of plasmids used in the various experiments are indicated in the figures and figure legends. After 24-h incubation in the dark, tobacco protoplasts were harvested and the α-amylase activity in the medium and in the cells was calculated according to the well established procedure described in Ref. (51).

Co-transfection practice using dual expression vectors

For transient expression in tobacco leaf protoplasts, all pFB62-based dual expression vectors were first tested individually by monitoring expression levels of the internal Golgi marker ST-YFP via western blotting to normalize transfection efficiencies. Under these conditions, the effect of different Rab GTPases and derived mutants could be compared in a quantitative and reproducible manner. Co-transfection of plasmids encoding the soluble vacuolar cargo molecules derived from barley α-amylase with the dual vectors were tested again for ST-YFP expression as additional quality control. Differences in the effect of RabGTPases expressed from the same plasmid could thus be attributed to the nature of the GTPases themselves rather than variance in transfection efficiency.

Tobacco leaf infiltration procedure and confocal laser scanning microscopy

Nicotiana tabacum cv Petit Havana SR1 (48) grown in soil were used for *A. tumefaciens*-mediated leaf infiltration. Agrobacterium cultures of strains harbouring the desired plasmids were adjusted to an OD of 0.1 (52). A square of around 0.5 × 0.5 cm was cut from the infiltrated area and used for confocal microscopy analysis. The material was mounted on a glass slide with the lower epidermis facing up the cover glass (22 mm × 50 mm, N. 0). Figures 1, 5 and Figure S1 were generated with an inverted Zeiss LSM 700 Laser Scanning Microscope (Zeiss). When the GFP/YFP/VENUS and RFP combination was used samples were excited with a diode laser at the wavelength of 488 nm for GFP/YFP/VENUS and 555 nm for RFP. Fluorescence was detected with a 552 nm dichroic beam splitter and a 475–550 nm bandpass filter for GFP/YFP/VENUS and a 560–700 nm bandpass filter for RFP.

Figure 2 and Figures S2 and S3 were generated with an upright Zeiss LSM 510 META Laser Scanning Microscope (Zeiss) with a Plan-Neofluar 40×/1.3 Oil DIC objective. The GFP and YFP combination samples were excited with an argon ion laser at the wavelength of 458 nm for GFP and 514 nm for YFP. Fluorescence was detected with a 545-nm dichroic beam splitter and a 480–520 nm bandpass filter for GFP and 565–615 nm for YFP. The GFP/YFP and RFP combination samples were excited with an argon ion laser at the wavelength of 488 nm for GFP or YFP and 543 nm for RFP. Fluorescence was detected with a 545-nm dichroic beam splitter and a 500–530 nm bandpass filter for GFP or YFP and 565–615 nm for RFP. Post-acquisition image processing was performed with LSM 5 image browser (Zeiss) and ImageJ (http://rsbweb.nih.gov/ij/).

Co-transformation practice for in situ *expression using dual expression vectors*

Unlike experiments with protoplast populations in which samples are averages of many cells, *in situ* fluorescent imaging is carried out on individual cells displaying variable levels of expression and co-expression. The dual expression vectors derived from pTFB62 for Agrobacterium-mediated leaf transformation were used to restrict analysis to only those cells expressing the internal marker as well as the cargo molecule to be influenced. Expression of the internal marker guarantees expression of the GTPase as effector as it is encoded by the same T-DNA. Moreover, using a constant laser output and detector gain, cells could be selected that express comparable levels of internal marker and thus GTPase for comparisons. Under these conditions, differences observed in the effect of various GTPases could thus be attributed to the nature of the GTPases, rather than co-expression efficiency.

Acknowledgments

F. B. was supported by a University of Leeds International research scholarship. The work in this article was in part supported by the European Union (project LSH-2002-1.2.5-2 'Recombinant Pharmaceuticals from Plant for Human Health Pharma-Planta') and by The Leverhulme Trust (F/10 105/E).

Supporting Information

Additional Supporting Information may be found in the online version of this article:

Figure S1: Comparison of CaMV35S- and TR2′-promoters (A) The plasma membrane marker YFP-SYP121 was expressed from the CaMV35S promoter or the TR2′-promoter by Agrobacterium-mediate tobacco leaf transformation, followed by an incubation of 48 h. Leaves were imaged at low magnification (10×) using a single microscope setting, and four random leaf areas were imaged for both promoter fusions. Notice the drastic reduction in fluorescence observed for TR2′-YFP-SYP121 compared to the corresponding CaMV35S promoter fusion. B) In order to compare CaMV35S promoter driven expression with TR2′-promoter controlled expression in a quantitative manner, promoter-reporter fusions were integrated into the tobacco genome by Agrobacterium-mediate T-DNA insertion, followed by regeneration of individual transgenic plant lines. Leaves from 15 independent transgenic lines for each chimeric gene were extracted, extracts normalized for total protein levels and analysed by the colorimetric GUS enzyme assay. The panel shows individual activities given in arbitrary units relative to the average GUS activity calculated for the fifteen CaMV35S-GUS plants which was set to 100 (±3.18). This resulted in an approximately 10-fold lower average value for the TR2′-GUS constructs yielding an average of just 11.26 (±0.41).

Figure S2: When expressed at low levels VENUS-Rha1 and Ara6-GFP do not label the TGN. Tobacco leaves were co-infiltrated with Agrobacterium strains harboring RFP- or YFP-tagged YFP-Syp61 together with either TR2-driven VENUS-Rha1 (A) or Ara6-RFP (B) encoding strains. VENUS-Rha1 or Ara6-RFP labelled structures that were always separate from the TGN marker Syp61, giving rise to negative Spearman correlation coefficients (r_S). Scale bars are 5 μm.

Figure S3: Regardless of expression levels GFP-Rha1 and Ara6-GFP do not label the Golgi. Tobacco leaves were co-infiltrated with Agrobacterium strains harbouring the Golgi marker ST-YFP or ST-CFP (indicated) together with TR2′-driven Venus-Rha1 (A), TR2′-driven Ara6-GFP (B), CaMV35S-driven GFP-Rha1 (C) or CaMV35S-driven Ara6-GFP (D). Under all conditions, the Golgi apparatus shows normal morphology and there is no significant correlation with the Rab5 fusions. Scale bars are 5 μm.

Figure S4: TGN and PVC are still distinct in the presence of nucleotide-free Rab5s and Rab7. Tobacco leaves were co-infiltrated with an Agrobacterium strain harbouring a GFP-VSR2 plasmid together with dual expression plasmids for the simultaneous expression of the TGN marker YFP-Syp61 and either PAT (A), Rha1(NI) (B), Ara6(NI) (C) or Rab7(NI) (D). Expression of Rha1, Ara6 and Rab7 mutants does not lead to TGN–PVC fusion. Scale bars are 5 μm.

Figure S5: Oligonucleotide pairs used in this study.

Please note: Wiley-Blackwell are not responsible for the content or functionality of any supporting materials supplied by the authors. Any queries (other than missing material) should be directed to the corresponding author for the article.

References

1. Marty F. Plant vacuoles. Plant Cell 1999;11:587–600.
2. daSilva LL, Foresti O, Denecke J. Targeting of the plant vacuolar sorting receptor BP80 is dependent on multiple sorting signals in the cytosolic tail. Plant Cell 2006;18:1477–1497.
3. daSilva LL, Taylor JP, Hadlington JL, Hanton SL, Snowden CJ, Fox SJ, Foresti O, Brandizzi F, Denecke J. Receptor salvage from the prevacuolar compartment is essential for efficient vacuolar protein targeting. Plant Cell 2005;17:132–148.
4. Kirsch T, Paris N, Butler JM, Beevers L, Rogers JC. Purification and initial characterization of a potential plant vacuolar targeting receptor. Proc Natl Acad Sci USA 1994;91:3403–3407.
5. Shimada T, Fuji K, Tamura K, Kondo M, Nishimura M, Hara-Nishimura I. Vacuolar sorting receptor for seed storage proteins in *Arabidopsis thaliana*. Proc Natl Acad Sci USA 2003;100:16095–16100.
6. Craddock CP, Hunter PR, Szakacs E, Hinz G, Robinson DG, Frigerio L. Lack of a vacuolar sorting receptor leads to non-specific missorting of soluble vacuolar proteins in Arabidopsis seeds. Traffic 2008;9:408–416.
7. Foresti O, Gershlick DC, Bottanelli F, Hummel E, Hawes C, Denecke J. A recycling-defective vacuolar sorting receptor reveals an intermediate compartment situated between prevacuoles and vacuoles in tobacco. Plant Cell 2010;22:3992–4008.
8. Bucci C, Parton RG, Mather IH, Stunnenberg H, Simons K, Hoflack B, Zerial M. The small GTPase rab5 functions as a regulatory factor in the early endocytic pathway. Cell 1992;70:715–728.
9. Sohn EJ, Kim ES, Zhao M, Kim SJ, Kim H, Kim YW, Lee YJ, Hillmer S, Sohn U, Jiang L, Hwang I. Rha1, an Arabidopsis Rab5 homolog, plays a critical role in the vacuolar trafficking of soluble cargo proteins. Plant Cell 2003;15:1057–1070.
10. Bolte S, Brown S, Satiat-Jeunemaitre B. The N-myristoylated Rab-GTPase m-Rabmc is involved in post-Golgi trafficking events to the lytic vacuole in plant cells. J Cell Sci 2004;117:943–954.
11. Kotzer AM, Brandizzi F, Neumann U, Paris N, Moore I, Hawes C. AtRabF2b (Ara7) acts on the vacuolar trafficking pathway in tobacco leaf epidermal cells. J Cell Sci 2004;117:6377–6389.
12. Bottanelli F, Foresti O, Hanton S, Denecke J. Vacuolar transport in tobacco leaf epidermis cells involves a single route for soluble cargo and multiple routes for membrane cargo. Plant Cell 2011; 23:3007–3025.
13. Saito C, Ueda T, Abe H, Wada Y, Kuroiwa T, Hisada A, Furuya M, Nakano A. A complex and mobile structure forms a distinct subregion

within the continuous vacuolar membrane in young cotyledons of Arabidopsis. Plant J 2002;29:245–255.
14. Limpens E, Ivanov S, van Esse W, Voets G, Fedorova E, Bisseling T. Medicago N2-fixing symbiosomes acquire the endocytic identity marker Rab7 but delay the acquisition of vacuolar identity. Plant Cell 2009;21:2811–2828.
15. Ueda T, Yamaguc M, Uchimiya H, Nakano A. Ara6, a plant-unique novel type Rab GTPase, functions in the endocytic pathway of Arabidopsis thaliana. EMBO J 2001;20:4730–4741.
16. Dacks JB, Poon PP, Field MC. Phylogeny of endocytic components yields insight into the process of nonendosymbiotic organelle evolution. Proc Natl Acad Sci USA 2008;105:588–593.
17. Lee GJ, Sohn EJ, Lee MH, Hwang I. The Arabidopsis rab5 homologs rha1 and ara7 localize to the prevacuolar compartment. Plant Cell Physiol 2004;45:1211–1220.
18. Ueda T, Uemura T, Sato MH, Nakano A. Functional differentiation of endosomes in Arabidopsis cells. Plant J 2004;40:783–789.
19. Ebine K, Fujimoto M, Okatani Y, Nishiyama T, Goh T, Ito E, Dainobu T, Nishitani A, Uemura T, Sato MH, Thordal-Christensen H, Tsutsumi N, Nakano A, Ueda T. A membrane trafficking pathway regulated by the plant-specific RAB GTPase ARA6. Nat Cell Biol 2011;13:853–859.
20. Goh T, Uchida W, Arakawa S, Ito E, Dainobu T, Ebine K, Takeuc M, Sato K, Ueda T, Nakano A. VPS9a, the common activator for two distinct types of Rab5 GTPases, is essential for the development of *Arabidopsis thaliana*. Plant Cell 2007;19:3504–3515.
21. Haas TJ, Sliwinski MK, Martinez DE, Preuss M, Ebine K, Ueda T, Nielsen E, Odorizzi G, Otegui MS. The Arabidopsis AAA ATPase SKD1 is involved in multivesicular endosome function and interacts with its positive regulator LYST-INTERACTING PROTEIN5. Plant Cell 2007;19:1295–1312.
22. Gruenberg J, Stenmark H. The biogenesis of multivesicular endosomes. Nat Rev Mol Cell Biol 2004;5:317–323.
23. Velten J, Velten L, Hain R, Schell J. Isolation of a dual plant promoter fragment from the Ti plasmid of *Agrobacterium tumefaciens*. EMBO J 1984;3:2723–2730.
24. French AP, Mills S, Swarup R, Bennett MJ, Pridmore TP. Colocalization of fluorescent markers in confocal microscope images of plant cells. Nat Protoc 2008;3:619–628.
25. Pimpl P, Hanton SL, Taylor JP, Pinto-DaSilva LL, Denecke J. The GTPase ARF1p controls the sequence-specific vacuolar sorting route to the lytic vacuole. Plant Cell 2003;15:1242–1256.
26. Brandizzi F, Snapp EL, Roberts AG, Lippincott-Schwartz J, Hawes C. Membrane protein transport between the endoplasmic reticulum and the Golgi in tobacco leaves Is energy dependent but cytoskeleton independent: evidence from selective photobleaching. Plant Cell 2002;14:1293–1309.
27. Jones S, Litt RJ, Richardson CJ, Segev N. Requirement of nucleotide exchange factor for Ypt1 GTPase mediated protein transport. J Cell Biol 1995;130:1051–1061.
28. Jones S, Newman C, Liu F, Segev N. The traPP complex is a nucleotide exchanger for Ypt1 and Ypt31/32. Mol Biol Cell 2000;11:4403–4411.
29. Richardson CJ, Jones S, Litt RJ, Segev N. GTP hydrolysis is not important for Ypt1 GTPase function in vesicular transport. Mol Cell Biol 1998;18:827–838.
30. Munder T, Furst P. The *Saccharomyces cerevisiae* CDC25 gene product binds specifically to catalytically inactive ras proteins *in vivo*. Mol Cell Biol 1992;12:2091–2099.
31. Uemura T, Ueda T, Ohniwa RL, Nakano A, Takeyasu K, Sato MH. Systematic analysis of SNARE molecules in Arabidopsis: dissection of the post-Golgi network in plant cells. Cell Struct Funct 2004;29:49–65.
32. Wurmser AE, Sato TK, Emr SD. New component of the vacuolar class C-Vps complex couples nucleotide exchange on the Ypt7 GTPase to SNARE-dependent docking and fusion. J Cell Biol 2000;151: 551–562.
33. Nordmann M, Cabrera M, Perz A, Brocker C, Ostrowicz C, Engelbrecht-Vandre S, Ungermann C. The Mon1-Ccz1 complex is the GEF of the late endosomal Rab7 homolog Ypt7. Curr Biol 2010;20:1654–1659.
34. Phillipson BA, Pimpl P, daSilva LL, Crofts AJ, Taylor JP, Movafeghi A, Robinson DG, Denecke J. Secretory bulk flow of soluble proteins is efficient and COPII dependent. Plant Cell 2001;13:2005–2020.
35. Batoko H, Zheng H-Q, Hawes C, Moore I. A Rab1 GTPase is required for transport between the endoplasmic reticulum and golgi apparatus and for normal golgi movement in plants. Plant Cell 2000;12:2201–2217.
36. Stenmark H. Rab GTPases as coordinators of vesicle traffic. Nat Rev Mol Cell Biol 2009;10:513–525.
37. Pinheiro H, Samalova M, Geldner N, Chory J, Martinez A, Moore I. Genetic evidence that the higher plant Rab-D1 and Rab-D2 GTPases exhibit distinct but overlapping interactions in the early secretory pathway. J Cell Sci 2009;122:3749–3758.
38. Wang J, Cai Y, Miao Y, Lam SK, Jiang L. Wortmannin induces homotypic fusion of plant prevacuolar compartments. J Exp Bot 2009;60:3075–3083.
39. Barbacid M. ras genes. Annu Rev Biochem 1987;56:779–827.
40. Sato M, Sato K, Fonarev P, Huang CJ, Liou W, Grant BD. *Caenorhabditis elegans* RME-6 is a novel regulator of RAB-5 at the clathrin-coated pit. Nat Cell Biol 2005;7:559–569.
41. Semerdjieva S, Shortt B, Maxwell E, Singh S, Fonarev P, Hansen J, Schiavo G, Grant BD, Smythe E. Coordinated regulation of AP2 uncoating from clathrin-coated vesicles by rab5 and hRME-6. J Cell Biol 2008;183:499–511.
42. Horiuc H, Lippe R, McBride HM, Rubino M, Woodman P, Stenmark H, Rybin V, Wilm M, Ashman K, Mann M, Zerial M. A novel Rab5 GDP/GTP exchange factor complexed to Rabaptin-5 links nucleotide exchange to effector recruitment and function. Cell 1997;90:1149–1159.
43. Peralta ER, Martin BC, Edinger AL. Differential effects of TBC1D15 and mammalian Vps39 on Rab7 activation state, lysosomal morphology, and growth factor dependence. J Biol Chem 2010;285:16814–16821.
44. Foresti O, Denecke J. Intermediate organelles of the plant secretory pathway: identity and function. Traffic 2008;9:1599–1612.
45. Phillipson BA, Pimpl P, Lamberti Pinto daSilva L, Crofts AJ, Taylor JP, Movafeghi A, Robinson DG, Denecke J. Secretory bulk flow of soluble proteins is efficient and COPII dependent. Plant Cell 2001;13:2005–2020.
46. Snowden CJ, Leborgne-Castel N, Wootton LJ, Hadlington JL, Denecke J. *In vivo* analysis of the lumenal binding protein (BiP) reveals multiple functions of its ATPase domain. Plant J 2007;52:987–1000.
47. Denecke J, De Rycke R, Botterman J. Plant and mammalian sorting signals for protein retention in the endoplasmic reticulum contain a conserved epitope. EMBO J 1992;11:2345–2355.
48. Maliga P, Sz-Breznovits A, Marton L. Streptomycin-resistant plants from callus culture of haploid tobacco. Nat New Biol 1973;244:29–30.
49. Murashige R, Skoog F. A revised medium for rapid growth and bioassays with tobacco tissue cultures. Physiol Plant 1962;15:473–497.
50. Hadlington JL, Denecke J. Sorting of soluble proteins in the secretory pathway of plants. Curr Opin Plant Biol 2000;3:461–468.
51. Foresti O, Dasilva LL, Denecke J. Overexpression of the Arabidopsis syntaxin PEP12/SYP21 inhibits transport from the prevacuolar compartment to the lytic vacuole *in vivo*. Plant Cell 2006;18:2275–2293.
52. Sparkes IA, Runions J, Kearns A, Hawes C. Rapid, transient expression of fluorescent fusion proteins in tobacco plants and generation of stably transformed plants. Nat Protoc 2006;1:2019–2025.